




Article

Characterization of Bioadsorbents from Organic Municipal Waste

Marcelina Sołtysik , Izabela Majchrzak-Kuceba  and Dariusz Wawrzyńczak 

Department of Advanced Energy Technologies, Faculty of Infrastructure and Environment, Czestochowa University of Technology, Dabrowskiego Street 73, 42-201 Czestochowa, Poland; izabela.majchrzak-kuceba@pcz.pl (I.M.-K.); dariusz.wawrzynczak@pcz.pl (D.W.)

* Correspondence: marcelina.soltysik@pcz.pl

Abstract: This article describes the production of bioadsorbents coming from seven different kinds of organic waste, produced in huge quantities in households, in a two-stage process. In order to determine the influence of the process parameters of carbonization (I stage) and activation with potassium hydroxide solution (II stage), the following analysis of the physicochemical properties of each sample at each stage processing was performed: base elemental composition, structure properties, surface morphology, thermal stability, crystallinity, and transmittance spectra characteristic bands. There was a lack of research on samples after each stage of waste processing in the literature. Addressing this allowed us to evaluate the transformative potential of each kind of organic waste included in the research and select the best waste for the production of bioadsorbents commonly used in environmental protection. Moreover, the results were compared with the ones in the literature. The utilization of particular kinds of organic waste seems to be especially important taking into account the strategy of waste management and sustainable development.

Keywords: bioadsorbent; activated carbon; biocarbon; biowaste; biomass; chemical activation; waste management; circular economy



Citation: Sołtysik, M.; Majchrzak-Kuceba, I.; Wawrzyńczak, D. Characterization of Bioadsorbents from Organic Municipal Waste. *Materials* **2024**, *17*, 1954. <https://doi.org/10.3390/ma17091954>

Academic Editor: Valery N. Khabashesku

Received: 16 March 2024
Revised: 12 April 2024
Accepted: 17 April 2024
Published: 23 April 2024



Copyright: © 2024 by the authors. Licensee MDPI, Basel, Switzerland. This article is an open access article distributed under the terms and conditions of the Creative Commons Attribution (CC BY) license (<https://creativecommons.org/licenses/by/4.0/>).

1. Introduction

The quantity of municipal waste produced is on the rise, presenting a significant global challenge. In 2022, Poland recorded 355 kg of garbage per capita, which means a decrease of 5 kg compared to the previous year. In Europe, on average, there is 513 kg of municipal waste per capita, based on Eurostat data for 2022 (data for 2023 is not yet available). Figure 1 provides a summary of per capita waste collection in European Union countries in 2022 [1]. Only 40% of the municipal waste is selectively collected, leaving the rest untreated in landfills. The European Union is firmly committed to a circular economy in its economic policy. This concept, prominently featured in EU waste documents, prioritizes the reuse of waste materials and their reintegration into circulation. The Bureau of International Recycling designates recyclables as the “seventh resource,” recognizing recycling material as one of the planet’s six essential resources, alongside water, air, oil, natural gas, coal, and ores [2]. According to Directive (EU) 2018/851, the goal is to recycle as much as 65% of waste by 2035, a target that is currently distant [3]. In Poland, the proposed European directive aligns with the draft of the National Waste Management Plan 2028 (KPGO), adopting the same requirements as the EU directive [4].

Disposing of municipal waste in landfills presents numerous drawbacks. These drawbacks encompass extensive spaces designated solely for handling substantial waste quantities, challenges in waste transportation and collection, potential environmental contamination, and the risk of groundwater and nearby water reservoir pollution. Additionally, landfill sites create conditions conducive to the growth of pathogenic microorganisms, the presence of rodents, and the potential transmission of pathogens by birds. Moreover, landfills contribute to the emission of CO₂ during the waste decomposition process [5].

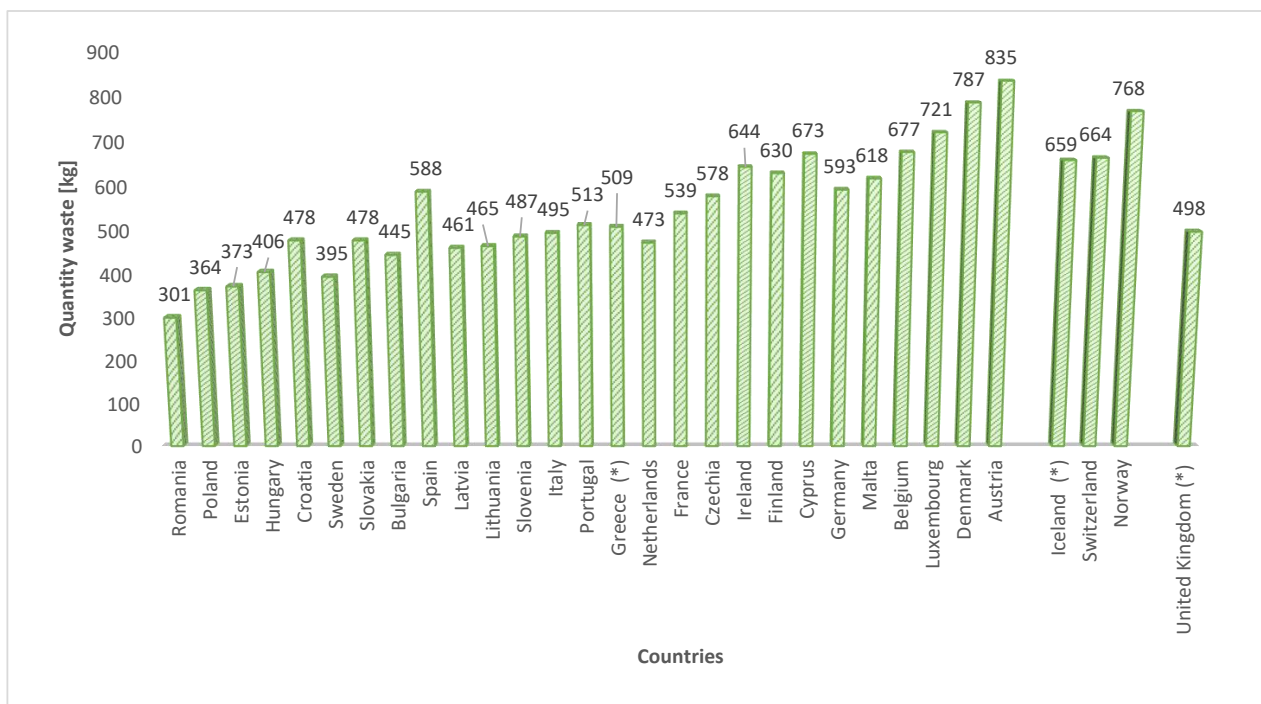


Figure 1. Municipal waste produced in the EU countries in kg per capita in 2022. * countries not belonging to the EU: Iceland and Norway (EEA countries) + Switzerland.

In addition, 27% of total waste is organic waste [6], which is why there is a growing interest in its utilization. One of the straightforward methods for managing organic waste involves its use as a natural fertilizer for reclaiming degraded soils. Some waste has also been repurposed as raw material for the manufacture of recycled items such as cups and pots. Additionally, it has found application in cosmetics production.

In Poland, over 13 million tons of municipal waste are generated annually [7]. The largest concentration of waste is located mainly in the southwestern part of Poland, covering an area of several thousand hectares. Approximately 1.7 billion tons of waste have already been deposited in landfills, of which approximately 43% concerns only the Silesian Voivodeship. Currently, the costs related to transport and storage amount to several billion dollars nationwide [5]. Waste processing is a key challenge today.

In Poland, the yearly production of waste includes 120,000 tons of coffee grounds and 103,000 tons of tea grounds [8,9]. Each Polish individual consumes approximately 36 kg of potatoes annually, resulting in peelings that contribute to about 24,000 tons of waste [10].

Kitchen waste is a great compost material. It can be used to enrich the soil, improve soil structure, and support the growth of plants in gardens or for agricultural purposes. Recycling kitchen waste into fertilizers reduces the need for synthetic fertilizers, contributing to sustainable agriculture. Organic waste, including coffee and tea grounds, can be utilized for bioenergy production through anaerobic digestion or biomass combustion. The fibers in coffee grounds can be extracted and combined with other materials to create clothing, accessories, or even biodegradable packaging. By finding innovative ways to repurpose and recycle organic waste from coffee and tea grounds and other kitchen scraps, communities can contribute to a more sustainable and circular approach to waste management.

Various organic waste can be employed to create bioadsorbents, encompassing agricultural residues like rice husks, coconut shells, and sugarcane bagasse, in addition to food and industrial waste. These waste types contain cellulose, lignin, and other complex compounds suitable as raw materials for bioadsorbent production. Several examples of bioadsorbents derived from organic waste are summarized in Table 1.

Table 1. Comparison of bioadsorbents' properties, which depend on raw material and production procedure.

| Raw Material | Coconut Shells | | Rice Husks | | Pomegranate Peels | Carrot Peels | Coffee Residue | |
|--|---|---|---|--|---|--|------------------------------------|--|
| annual production | >25 Mtons (Southeast Asia and the Asia-Pacific region) [11] | | ~700 Mtons (global production) [12,13] | | ~30 Mtons (global production) [14] | | ~15 Mtons (global production) [15] | |
| activation process | two-stage activation process involving urea and KOH [16] | single-stage physical activation process using carbon dioxide | two-stage activation process involving KOH and chitosan | single-stage activation the organic waste with KOH | one-stage activation with potassium hydroxide | activation with the same chemical compound | one-stage physical | one-stage chemical activation with KOH |
| adsorbent specific properties achieved | 1687 m ² /g 83% of C | 1357 m ² /g | 1500 m ² /g, 82% of C | 2695 m ² /g | 2144 m ² /g | 1376 m ² /g | 534 m ² /g 82% of C | 840 m ² /g |
| Ref. | [16] | [17] | [18] | [19] | [20] | [21] | [22] | [23] |

Researchers primarily focus on the investigation of bioadsorbents, neglecting the comparison of their properties before modification. In the two-step process of acquiring bioadsorbents, it is crucial to assess their characteristics both prior to and after modification. This evaluation provides insights into various aspects, including the effectiveness of the modification procedure. However, there is an absence of such information in the existing literature, with bioadsorbents being characterized solely after undergoing modification. In addition, articles frequently narrow their focus to a specific type of waste, creating difficulties in comparing the properties of waste generated under similar conditions.

This article delivers a thorough analysis of waste materials, specifically bioadsorbents. The characterization was conducted at two key stages: after the carbonization phase and following the activation stage. The selected organic waste, commonly found in Central and Eastern Europe, encompassed coffee and tea waste, potato peelings, and both green and brown walnut shells. Notably, this study marked the inaugural utilization of green coffee waste and green walnut shells for the production of bioadsorbents.

2. Materials and Methods

2.1. Materials

The organic waste examined in this research was heavily roasted coffee residue, regular roasted coffee residue, potato peelings, tea residue, green walnut shells, and green coffee residue; this waste was chosen for its widespread presence and accessibility in Central and Eastern Europe. In order to maintain the purity of the selected materials for research purposes, they were obtained directly and separately after they were produced (not recovered from biowaste). Table 2 provides the labels assigned to each type of organic waste, as well as their designations after the carbonization and activation stages.

For the bioadsorbent preparation, two varieties of the widely consumed dark roasted coffee were employed.

The distinction between these two varieties arose from the distinct roasting processes they underwent: (1) HRoC, which underwent a dark roasting process conducted at temperatures ranging from 220 to 225 °C, possibly reaching 250 °C. This process led to dark brown or, in extreme cases, black beans, almost on the brink of charring. The high temperature in dark roasting tends to diminish caffeine and acidity. (2) RReC, which underwent light roasting at approximately 200 °C, resulting in a coffee with natural characteristics, high acidity, and elevated caffeine content.

Table 2. Designations of organic waste and products of their modification used in the article.

| No. | Organic Waste | Designation | Designation of Organic Waste after Carbonation | Designation of Organic Waste after Activation |
|-----|--------------------------------|-------------|--|---|
| 1. | Heavily roasted coffee residue | HRoC | CHRoC | AHRoC |
| 2. | Regular roasted coffee residue | RReC | CRRcC | ARRcC |
| 3. | Potato peelings | PP | CPP | APP |
| 4. | Tea residue | TR | CTR | ATR |
| 5. | Walnut green shells | WGS | CWGS | AWGS |
| 6. | Walnut shells | WS | CWS | AWS |
| 7. | Green coffee residue | GC | CGC | AGC |

Potato peelings (PP) were another material employed in the creation of biocarbons. Potatoes, a widely known plant since the 19th century in Europe and now globally recognized, come in numerous varieties, with Chilean varieties being particularly popular. The potato tuber consists of an inner tissue, typically yellow, enveloped by an outer thin casing of a darker color, slightly tougher than the inner subcutaneous tissue. Due to the somewhat earthy and bitter taste of potato skin, it is often removed before consuming the tuber. In the biocarbon preparation research, dried potato peelings were utilized as a substrate [24].

Residue from black tea (TR) brewing was collected after the extraction of tea essence during the tea infusion process. The descended tea residue, when re-infused with boiling water to create a tea beverage, exhibited no release of tea essence and no alteration in water color. The specific tea variety utilized for this purpose was a classic pure black tea sourced from Ceylon [25]. Upon drying the tea residue, it became exceedingly brittle, devoid of moisture, and retained its original brown color.

The walnut tree, belonging to the walnut family, is a deciduous tree species widely popular in Central and Eastern Europe, as well as across a vast expanse of Asia, the Balkans, the Himalayas, and China. Due to the preference for walnut fruits among birds, particularly those from the crow family, these fruits are often carried over long distances, with birds occasionally burying them in agricultural areas, contributing to their dispersal. Walnut trees boast remarkable longevity, capable of bearing fruit for up to 500 years. The walnut fruit comprises several layers, including the outer green pericarp, a soft covering for the woody shell formed internally. The seed, encased in a membranous shell and commonly known as the kernel, is the edible part of the fruit. In the research, two parts of the walnut fruit were employed. The green part (labeled as WGS), upon drying, lost its firmness and color, transforming into a brittle material with shades of brown and black. The other part, the woody shell (WS), exhibited no alteration in physical properties during drying, except for a reduction in weight due to the loss of a minimal amount of moisture [26].

The research also utilized coffee residue derived from green coffee (GC) as another material. Green coffee is characterized by the absence of roasting before being sold, resulting in harder and earthier qualities in the ground green coffee beans. The residue from green coffee is more resilient, and there is no discernible distinction between its appearance before and after use.

The kinds of dried organic waste described above are depicted in Figure 2a–f. The walnut green shells (WGS) and walnut shells (WS) are presented together as cohesive components (Figure 2e), even though they were subjected to separate processing in subsequent research.

The organic waste underwent a comprehensive cleaning process with tap water, followed by natural drying and further drying in an oven at 105 °C before undergoing carbonization. These dried precursors were subsequently ground into a powder form with dimensions in the range of a few millimeters.



Figure 2. The collected and pre-prepared organic waste, used for the preparation of bioadsorbents: (a) heavily roasted coffee residue, (b) regular roasted coffee residue (c) potato peelings, (d) tea residue, (e) walnut green shells and walnut shells, (f) green coffee residue.

2.2. Characterization of Materials

Elemental Analysis of the Samples

The chemical analysis of the organic waste involved both direct and indirect methods. Properties such as moisture content, carbon, hydrogen, nitrogen, and sulfur content were determined. Moisture content in the samples was assessed using the weight-dryer method with a laboratory dryer (SLW 11 with forced air circulation), following the PN-EN ISO 18134-1 standard [27].

Figure 3 illustrates the mass losses observed at each stage of bioadsorbent preparation. Notably, in the case of coffee residue, there is a noticeable weight reduction during the drying process. This is attributed to the small, dense grain size and the hygroscopic nature of coffee residue, making exclusive air drying impractical. The greater the mass loss during carbonization and activation, the higher the specific surface area of the resulting bioadsorbents. In the case of APP, ATR, and AGC, the mass after activation increased. The final ash weight (above 10%) may indicate poor rinsing of the adsorbent from the activator.

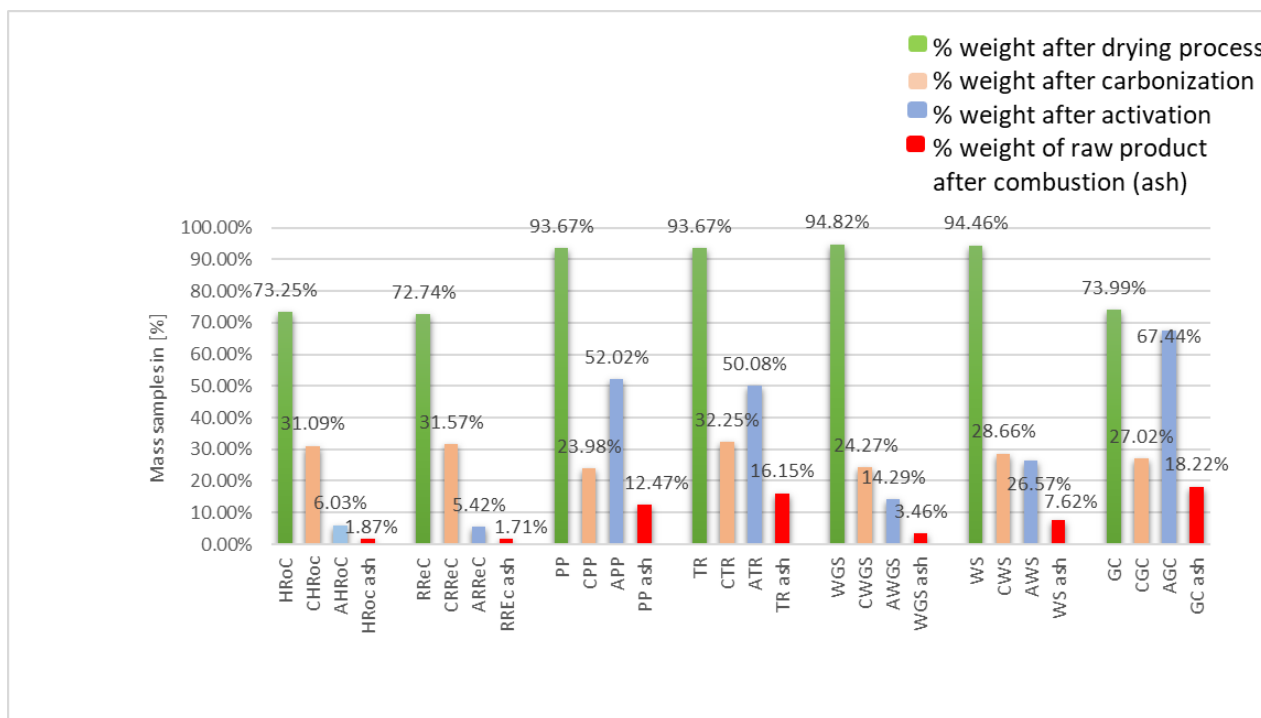


Figure 3. Residual weight of samples by percent at each stage of their processing.

The elemental composition of organic waste, i.e., the determination of the content of carbon, hydrogen, nitrogen, and sulfur, was performed using the LECO Truspec CHNS analyzer. The tests were carried out for samples in a dry state, that were ground into particles less than 0.2 mm in size, in accordance with the requirements of the standard PN-EN ISO 16948:2015-07 [28]. Oxygen was calculated by difference.

Table 3 is a summary of the obtained analysis results for the organic waste used. All materials are characterized by high carbon content and sulfur content. These features are demonstrated by properly selected materials for obtaining carbon materials [29]. The elemental composition of the organic municipal waste subjected to the tests corresponds to the range given in the literature [30–32].

Table 3. Chemical characterization of organic municipal waste.

| Sample | Unit | HRoC | RReC | PP | TR | WGS | WS | GC |
|---------|------|------|-------|-------|-------|-------|-------|-------|
| Element | C | wt.% | 44.75 | 48.59 | 42.85 | 43.93 | 43.94 | 38.82 |
| | H | wt.% | 5.88 | 6.31 | 5.89 | 5.43 | 5.38 | 5.60 |
| | N | wt.% | 2.08 | 2.32 | 2.37 | 2.89 | 0.77 | 1.72 |
| | S | wt.% | 0.00 | 0.01 | 0.05 | 0.08 | 0.01 | 0.09 |
| | O | wt.% | 47.29 | 42.77 | 49.34 | 49.83 | 49.90 | 48.48 |

3. Results and Discussions

3.1. Synthesis Bioadsorbents

The modification of the organic waste occurred through two stages: (I) carbonization and (II) activation. Stage I comprises 5 steps: (1) heating the organic waste at the rate of 5 °C/min up to 105 °C, (2) a 12 h period of soaking in a vacuum dryer at 105 °C, (3) heating the samples at the rate of 6 °C/min up to 700 °C in a muffle furnace in a nitrogen gas atmosphere, (4) conducting carbonization at a temperature of 700 °C for 0.75 h, and (5) cooling the sample to 25 °C with the rate of 6 °C/min. Stage II—activation, involves 6 steps: (1) saturating the sample for 2 h with a pre-prepared KOH solution (1 mol), where the solution-to-sample ratio was 2:1, (2) heating samples from 25 to 105 °C in an oven, (3) drying the samples for 12 h in a vacuum dryer at 105 °C, (4) heating the samples at the rate of 6 °C/min

up to 700 °C in a muffle furnace in a nitrogen gas atmosphere, (5) activating at a temperature of 700 °C for 0.75 h at a heating rate of 3 °C/min, and (6) cooling the sample to 25 °C (Figure 4).

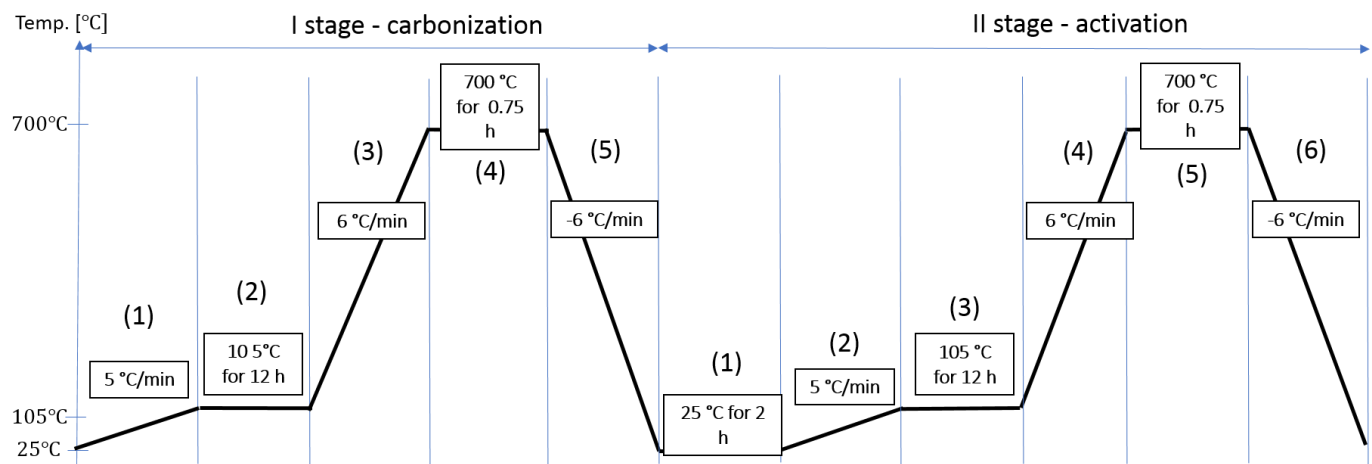


Figure 4. Procedure for the synthesis of bioadsorbents by modifying organic waste.

The solid bioadsorbents obtained from the activation were washed with distilled water until achieving a neutral pH. The resulting bioadsorbents were then dried at 120 °C for 12 h.

3.2. Characterization of Materials

The LECO TruSpec CHN/S analyzer was employed to assess the C, H, N, S, and O contents in the samples following carbonization and activation, as described for organic waste in Section 2.1. The samples' material underwent degassing at 105 °C for 12 h to eliminate moisture or volatile impurities. Nitrogen adsorption isotherms at −196 °C were determined, covering relative pressures (p/p_0) from 0 to 0.98 across a broad range of pores. Due to the cryogenic temperature, N₂ diffusion was restricted in ultra-micropores (<0.7 nm). The surface area of the samples was computed using the Brunauer-Emmett-Teller (BET) equations, and the total pore volumes were calculated based on the adsorbed nitrogen amount at a relative pressure p/p_0 .

The morphology of the materials was investigated using a Carl Zeiss Microscopy GmbH scanning electron microscope (SEM model EVO 15). A vacuum in the range of 0.001–133 Pa and a magnification range of 5×–1,000,000× were required during the microscope chamber examination.

Thermogravimetric analysis (TGA) was conducted on a Mettler TGA/SDTA 851e thermobalance. The samples were initially purged with nitrogen and heated from 25 °C to 1000 °C at a constant heating rate of 10 °C/min.

XRD analysis was carried out to compare organic biomass samples with biomass samples post-carbonization and activation. Measurements were collected using copper radiation ($K\alpha_1 = 0.154056$ nm) in the 15–60 range on a 2θ scale. Scintillation counter angular speed was set at 0.0010/min, and the patterns were analyzed with Philips X'Pert, utilizing the X'Celerator Scientific detector.

The FTIR spectra of the activated organic municipal waste were recorded at room temperature using a Nicolet 6700 FT-IR spectrometer with the KBr pellet technique [33].

3.2.1. Characterization of Chemical Composition

Table 4 provides a summarized overview of the analysis results obtained for the various kinds of carbonized organic waste. Materials derived from walnut shells consist of almost 93% carbon. Coffee bean materials (CHRoC and CRReC) exhibit comparable high carbon content, ranging from 66% to 77%. Tea residue (CTR) shows approximately 72% carbon, while potato peelings (CPP) have around 61%. The lowest carbon content is found in walnut green shells (CWGS), accounting for less than 41%. A notable disparity in oxygen content following the carbonization process stems from the loss of the oxide group

during the heating stage. This loss of elemental oxygen is attributed to the volatilization of materials, particularly CO and CO₂ [34].

Table 4. Chemical composition of various carbonized materials from kinds of organic waste.

| Sample | Unit | CHRoC | CRRcC | CPP | CTR | CWGS | CWS | WGC | |
|---------|------|-------|-------|-------|-------|-------|-------|-------|-------|
| Element | C | wt.% | 66.69 | 77.04 | 61.20 | 72.76 | 40.72 | 95.58 | 69.80 |
| | H | wt.% | 1.31 | 1.55 | 1.22 | 1.47 | 1.26 | 1.39 | 1.24 |
| | N | wt.% | 2.92 | 3.88 | 2.23 | 2.95 | 0.69 | 0.58 | 2.73 |
| | S | wt.% | 0.00 | 0.01 | 0.01 | 0.06 | 0.01 | 0.00 | 0.06 |
| | O | wt.% | 29.08 | 17.52 | 34.34 | 22.76 | 57.32 | 5.45 | 26.17 |

Table 5 offers a concise overview of the analysis results derived from the activated organic waste (bioadsorbents). In these materials, a modest rise in carbon content is observed, accompanied by a more pronounced reduction in oxygen content. The nitrogen content undergoes essentially insignificant changes. The observable decrease in oxygen-combining compounds indicates further volatilization from the material. Meanwhile, the nearly unaltered nitrogen content during the activation process suggests the incorporation of nitrogen into the aromatic structure rather than in the functional groups on the layer edges [35].

Table 5. Chemical composition of various bioadsorbents obtained from kinds of organic waste.

| Sample | Unit | AHRoC | ARRcC | APP | ATR | AWGS | AWS | AGC | |
|---------|------|-------|-------|-------|-------|-------|-------|-------|-------|
| Element | C | wt.% | 68.89 | 79.90 | 63.44 | 72.59 | 45.56 | 93.52 | 76.41 |
| | H | wt.% | 1.84 | 1.78 | 3.13 | 2.04 | 2.18 | 2.18 | 1.59 |
| | N | wt.% | 5.36 | 6.23 | 2.40 | 3.82 | 3.11 | 3.38 | 2.89 |
| | S | wt.% | 0.00 | 0.00 | 0.00 | 0.01 | 0.00 | 0.00 | 0.02 |
| | O | wt.% | 23.91 | 12.09 | 31.03 | 21.54 | 49.15 | 0.92 | 19.09 |

3.2.2. BET Analysis

Table 6 includes the designated textural parameters and a brief explanation for the determined samples.

Table 6. Textural parameters determined from the adsorption isotherms of the studied samples.

| Textural Parameters | | |
|-------------------------|-----------|---|
| Total pore volume | V_p | Amount of N ₂ adsorbed at a relative pressure of 0.99 |
| Surface area | S_{BET} | Brunauer-Emmett-Teller equation [32] |
| Micropore volume | W_0 | N ₂ isotherms: Dubinin-Radushkevich (DR) equation assuming a density of the adsorbed phase of 0.808 cm ³ g ⁻¹ and a cross sectional area of 0.162 nm ² [36] |
| Average micropore width | L_0 | Stoeckli-Ballerini equation [37] |

The conducted N₂ adsorption isotherms helped to determine the texture parameters as total pore volume (V_p), pore size (S_{BET}), micropore size (W_0), and average micropore width (L_0) summarize Table 6. These analysis results enable a comparison of changes occurring in the samples of organic waste after the carbonization and activation processes. The texture parameters estimated from N₂ adsorption exhibit similar trends. The porosity develops in each material after the carbonization process and is particularly accentuated after the activation process. Pores within the range of 0.86–1.36 nm were achieved. The surface area increased from <1 m²/g for organic waste to 293 ÷ 1604 m²/g for activated bioadsorbents. The highest specific surface areas were attained for the activated potato peelings (1604 m²/g for APP) and roasted coffee residue (1580 m²/g for AHRoC). A slightly smaller pore surface was obtained for the activated sample of green walnut shells (AWGS—1376 m²/g). The same pattern applies to the volume of micropores, with the largest area

found in the activated roasted coffee residue (AHRoC-0.5 cm³/g) and the activated potato peelings (0.32 cm³/g for APP). However, in the case of the activated roasted coffee residue (AHRoC), the micropores were the smallest, with an average size of 0.96 nm. The accumulated electric charge, resulting from a large number of ions, caused the sample to adhere to the vessel walls, leading to difficulties in transferring the correct amount of sample and conducting measurements. Lack of parameters for biomass samples from walnut green shells (WGS) and green coffee residue (GC) arose from a poorly developed porous surface, rendering some parameter analyses impossible. The calculated beta area confirms such narrow porosity. The W_0 and L_0 values fall within the typical limits described by other authors, affirming the acquisition of microporous bioadsorbents [38,39].

Bioadsorbents obtained by other researchers have demonstrated comparable or inferior structural properties. For instance, Kim et al. achieved a biochar from coffee grounds through one-stage activation with potassium carbonate, yielding a surface area of 1692 m²/g [32]. Travis et al. obtained a bioadsorbent from coffee using two-stage activation of KOH, resulting in a specific surface area of 1624 m²/g [40]. Zhang et al. obtained a ZnCl₂ bioadsorbent from potato peelings with a specific surface area of 1604 m²/g [41]. For comparison, specific surfaces of other bioadsorbents reported in scientific articles are summarized in Table 7.

Table 7. Structural properties of samples.

| Sample | N ₂ Adsorption (at −196 ° C) | | | |
|--------|---|--------------------------------------|--------------------------------------|----------------------|
| | S _{BET} m ² /g | V _p cm ³ /g | W ₀ cm ³ /g | L ₀ nm |
| HRoC | 0.21 | 0.00006 | n/a | 1.54 |
| CHRoC | 18 | 0.008 | 0.004 | 1.36 |
| AHRoC | 1580 | 0.84 | 0.5 | 0.96 |
| RReC | 0.04 | 0.0024 | n/a | n/a |
| CRRcC | 37 | 0.02 | 0.01 | 1.6 |
| ARRcC | 863 | n/a | n/a | n/a |
| PP | 0.21 | 0.00005 | 0.00003 | 1.36 |
| CPP | 3.17 | 0.004 | 0.001 | 1.36 |
| APP | 1604 | 0.65 | 0.32 | 1.36 |
| TR | 0.52 | 0.0004 | 0.0002 | 1.60 |
| CTR | 115 | 0.05 | 0.02 | 1.27 |
| ATR | 564 | 0.25 | 0.12 | 0.86 |
| WGS | 0.62 | 0.00 | n/a | n/a |
| CWGS | 4.55 | 0.00 | 0.00 | 3.07 |
| AWGS | 1376 | 0.64 | 0.34 | 1.21 |
| WS | 0.17 | 0.0002 | 0.0001 | 1.6 |
| CWS | 289 | 0.12 | 0.12 | 0.93 |
| AWS | 416 | 0.20 | 0.18 | 0.86 |
| GC | n/a | n/a | n/a | n/a |
| CGC | 0.18 | 0.00013 | 0.00 | n/a |
| AGC | 293 | 0.12 | 0.05 | 1.18 |

Figure 5a–g display the N₂ adsorption and desorption isotherms for the samples. All activated samples (AHRoC, ARReC, APP, ATR, AWGS, AWS, and AGC) exhibit the International Union of Pure and Applied Chemistry (IUPAC) type I isotherm, indicating that the majority of N₂ is adsorbed at low pressures without the presence of hysteresis loops. This type I isotherm suggests that the adsorbent is predominantly composed of micropores [42,43]. With increasing severity in activation conditions (high activation temperature or prolonged activation time), there is a rise in N₂ adsorption uptake. Notably, the degree of N₂ adsorption increase is more pronounced when altering the activation temperature rather than the activation time. Nitrogen adsorption–desorption isotherms for

organic waste samples are nearly imperceptible, with adsorption being barely visible or entirely absent. Only the regular coffee residue (RReC) sample exhibits minimal adsorption ($<2 \text{ cm}^3/\text{g}$) and complete desorption. In the case of carbonized samples, visible adsorption–desorption is observed for the carbonized green walnut shell (CWGS) sample, reaching up to $4.5 \text{ cm}^3/\text{g}$. The carbonized walnut shell sample (CWS) displays high adsorption, up to $100 \text{ cm}^3/\text{g}$, but desorption is limited to $90 \text{ cm}^3/\text{g}$. For carbonized roasted and regular coffee residue (CHRoC, CRReC) samples, adsorption reaches up to 6 and $12 \text{ cm}^3/\text{g}$, respectively and desorption is complete. The carbonized tea residue (CTR) sample shows adsorption up to $4 \text{ cm}^3/\text{g}$ with complete desorption.

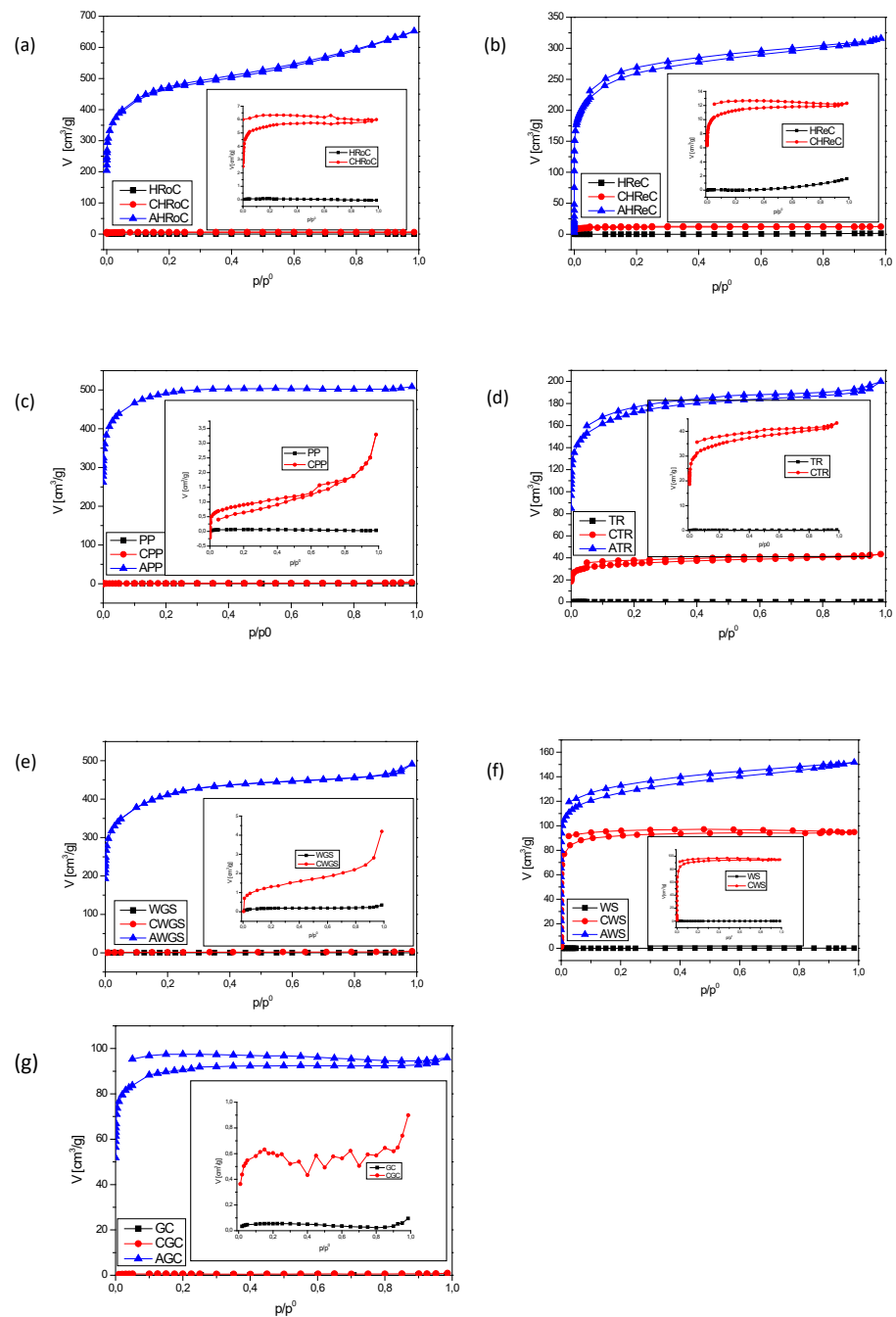


Figure 5. N_2 adsorption isotherms at $-196 \text{ }^\circ\text{C}$ of samples of organic waste after the carbonization process and after the activation process with (a) heavily roasted coffee residue, (b) regular roasted coffee residue, (c) potato peelings, (d) tea residue, (e) walnut green shells, (f) walnut shells, (g) green coffee residue.

In the case of the carbonized potato peeling (CPP) sample, adsorption reaches up to $3 \text{ cm}^3/\text{g}$ with nearly complete desorption. However, for the carbonized green coffee residue (CGC) sample, the adsorption–desorption data is unreliable.

Pore size distribution analysis was conducted to examine the textural properties of the samples. As depicted in Figure 6., the pore size distributions for non-activated samples after carbonization are similar, with minimal variations within the margin of error. Generally, these samples exhibit small porosity, which is negligible when compared to the activated samples. The smallest micropores, predominantly below 2 nm and in the highest concentration, are observed in the sample of activated roasted coffee (AHRoC). The absence of a curve for the lightly activated roasted coffee sample is attributed to challenges in working with the sample, which experiences significant electrification. Despite being already carbonized, the sample of regular coffee (CRReC) demonstrates a notable adsorption potential and a substantial number of micropores exceeding 2 nm. In the activated potato peeling sample (APP), the micropore peak is at 1.2 nm, while for the activated tea sample (ATG), it is at 0.8 nm, similar to the activated walnut shell sample (AWS) but with a higher concentration. The activated green walnut shell sample (AWGS) exhibits a broad range of micropores from 1.2 nm to 3.4 nm. Regarding microporosity, the samples of activated roasted coffee display the greatest potential, featuring a wide range of micropores and the highest concentration, surpassing the most developed microporosity observed in the sample.

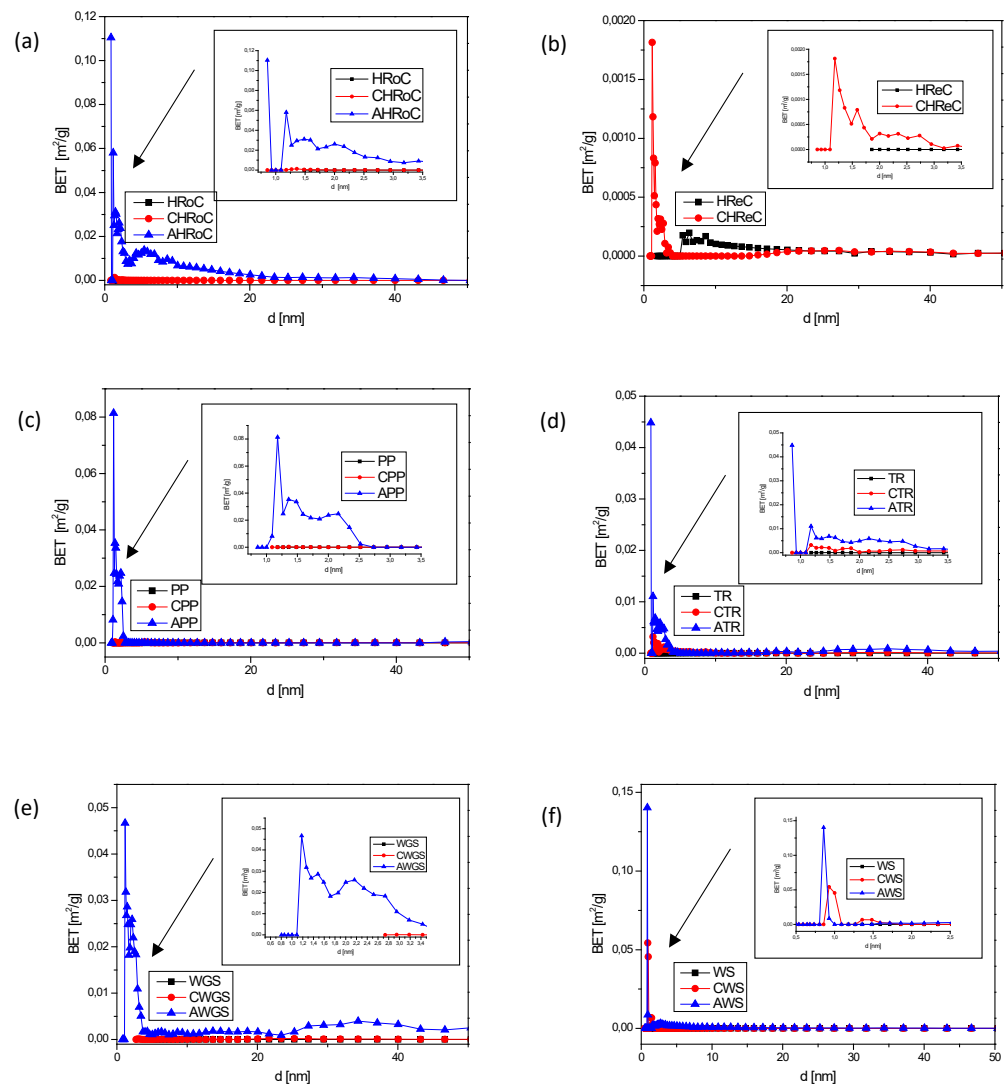


Figure 6. Cont.

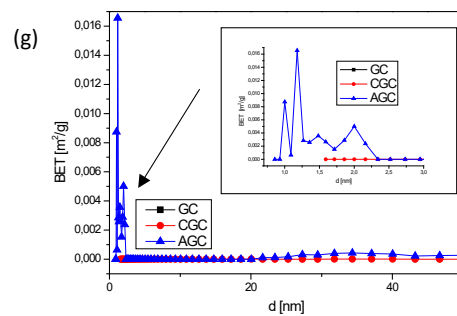


Figure 6. Pore size distributions of materials with (a) heavily roasted coffee residue, (b) regular roasted coffee residue, (c) potato peelings, (d) tea residue, (e) walnut green shells, (f) walnut shells, (g) green coffee residue.

3.2.3. SEM

Surface morphologies encompass the physical attributes and characteristics of a material's surface, including its shape, texture, roughness, and topography. To investigate the surface morphology of the materials, scanning electron microscopy (SEM) was employed [44]. SEM images were utilized to illustrate alterations in the internal structure of the samples at key stages of sample preparation [45]. Figures 7a, 8a, 9a, 10a, 11a, 12a and 13a present SEM images of organic waste samples HRoC, RReC, PP, TG, WGS, WS, and GC, while Figures 7b, 8b, 9b, 10b, 11b, 12b and 13b display carbonized organic waste samples CHRoC, CRReC, CPP, CTG, CWGS, CWS, and CGC. Activated organic waste (bioadsorbents) is depicted in Figures 7c, 8c, 9c, 10c, 11c, 12c and 13c—AHRoC, ARReC, APP, ATG, AWGS, AWS, and AGC. The SEM images captured during the examination reveal notable differences in the topography of the external structure of the materials. Even at the carbonization stage, and more prominently after the KOH activation process, substantial porosity becomes evident (images marked with “b”). Following the carbonization stage, macropores are observable in all materials (Figures 7b, 8b, 9b, 10b, 11b, 12b and 13b). In the case of bioadsorbents derived from coffee (AHRoC, ARReC), tea (ATG), and walnut shells (AWS), significant micropores are visible post-activation [46]. Samples of heavily roasted coffee (AHRoC) exhibit a very regular network of micropores after the activation process (Figure 7c). Slightly less regular but still significant microporous structures are observed in the sample of activated regular coffee (ARReC) (Figure 8c). The structure of the activated walnut shell sample (AWS) is noteworthy, featuring a network comprising both macro and micro pores (Figure 12c). The compiled photos of the samples were captured at the same magnification to facilitate better analysis and comparison.

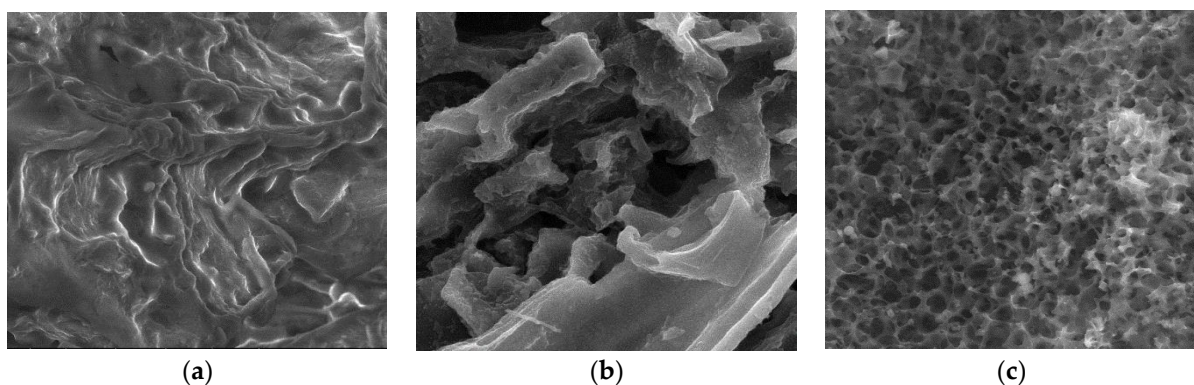


Figure 7. SEM images of (a) HRoC, (b) CHRoC, (c) AHRoC.

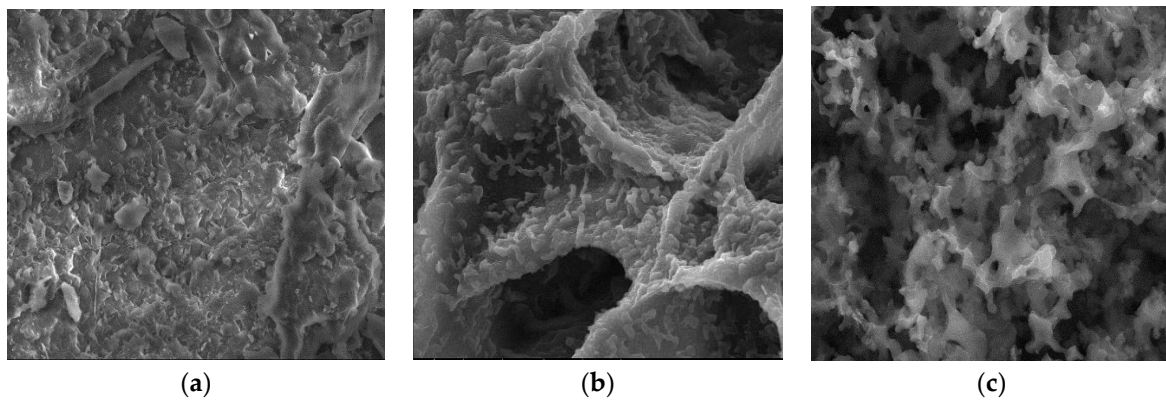


Figure 8. SEM images of (a) RReC, (b) CRRcC, (c) ARReC.

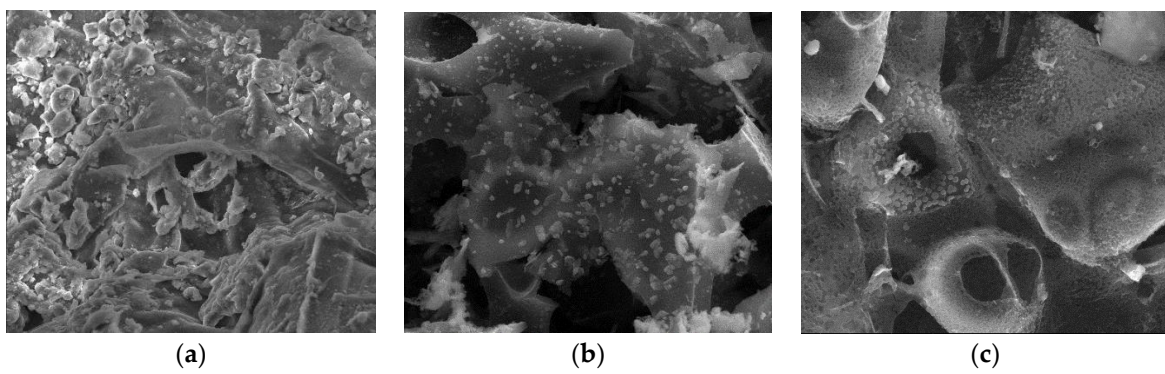


Figure 9. SEM images of (a) PP, (b) CPP, (c) APP.

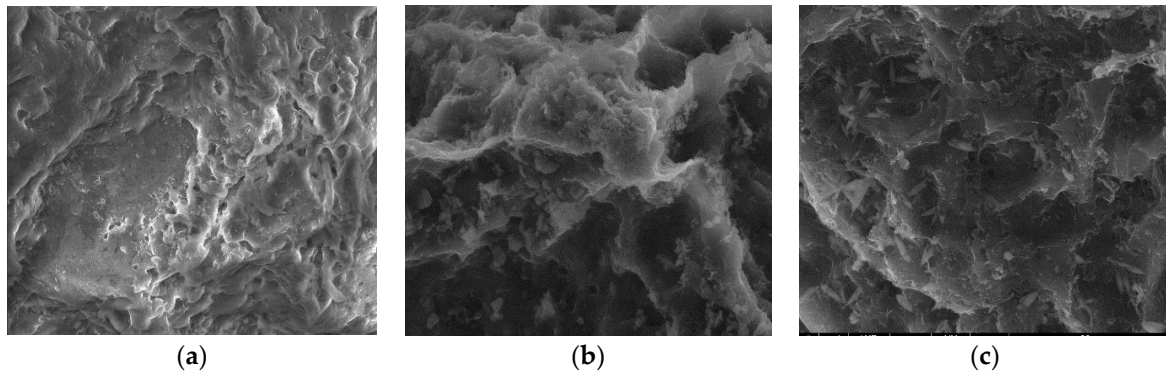


Figure 10. SEM images of (a) TR, (b) CTR, (c) ATR.

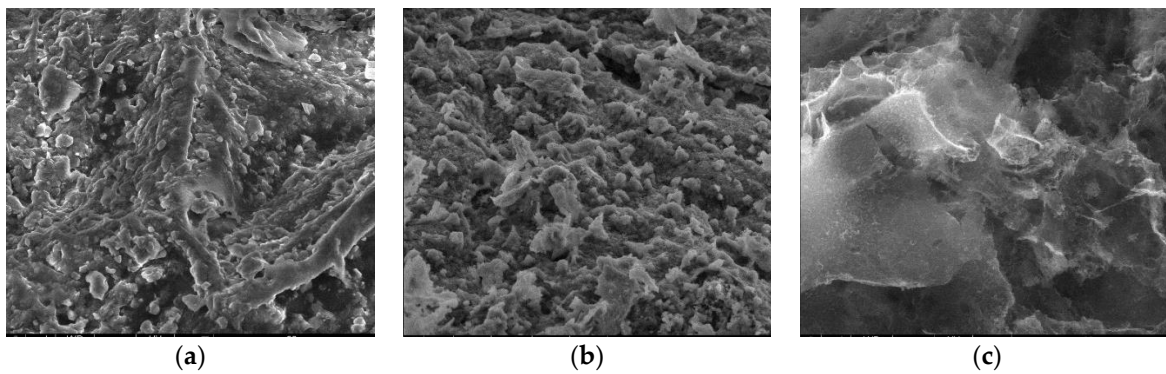


Figure 11. SEM images of (a) WGS, (b) CWGS, (c) AWGS.

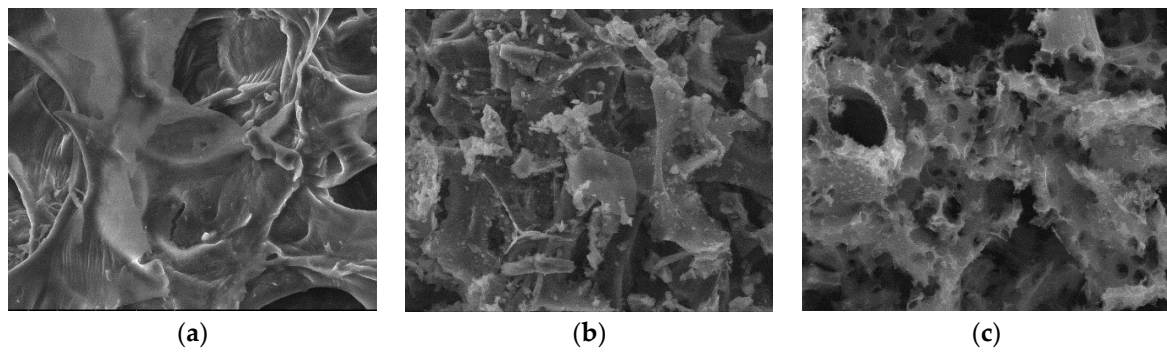


Figure 12. SEM images of (a) WS, (b) CWS, (c) AWS.

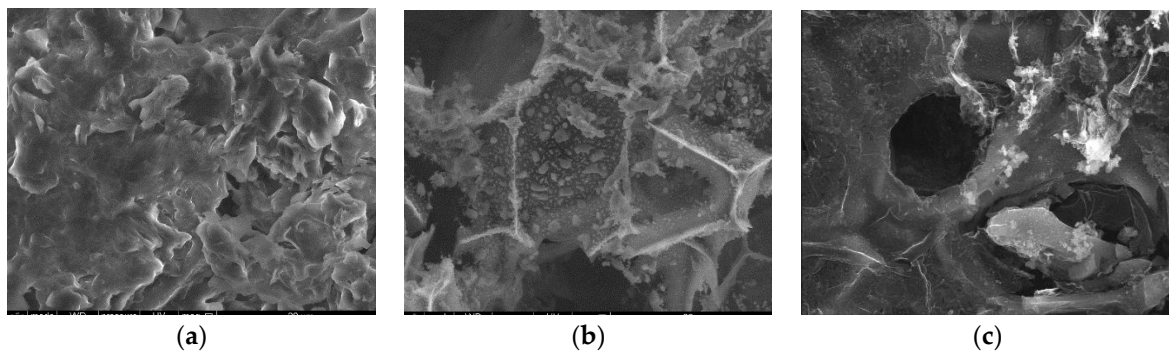


Figure 13. SEM images of (a) GC, (b) CGC, (c) AGC.

3.2.4. TG Profiles

An analysis of each sample of the materials was carried out to examine the thermal stability of materials at 25–1000 °C in a nitrogen atmosphere. In order to compare the changes occurring in the structures of the compounds in the modification processes, samples from the same kinds of waste are presented in the Figure 14. Common points of mass faults can be seen for dry biomass samples without modification. At 272 °C, hemicellulose degradation occurs, at 331 °C cellulose degradation occurs, and at 377 °C decomposition of lignin occurs [47]. In the case of samples after the carbonization and activation processes, a similarity can be found in the plots with a lower mass loss for the activated samples. The thermal stability of coffee samples after the activation process is reached much earlier, at about 450 °C. The weight loss around 600 °C for the activated coffee samples is attributed to skeletal condensation.

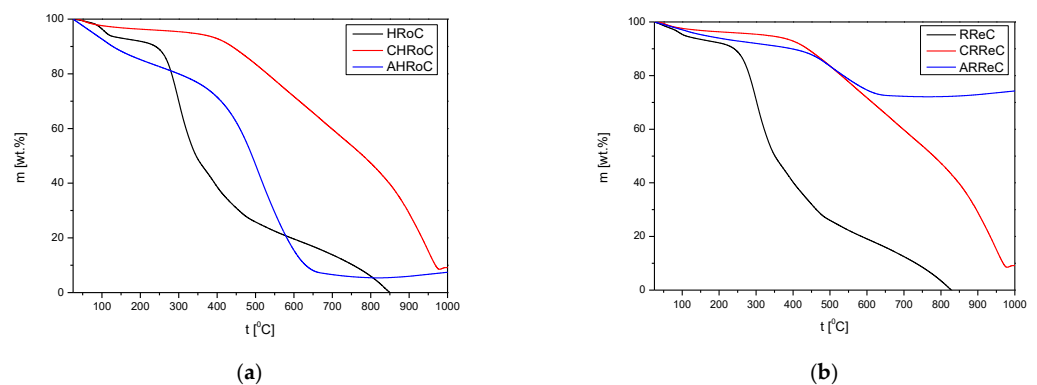


Figure 14. Cont.

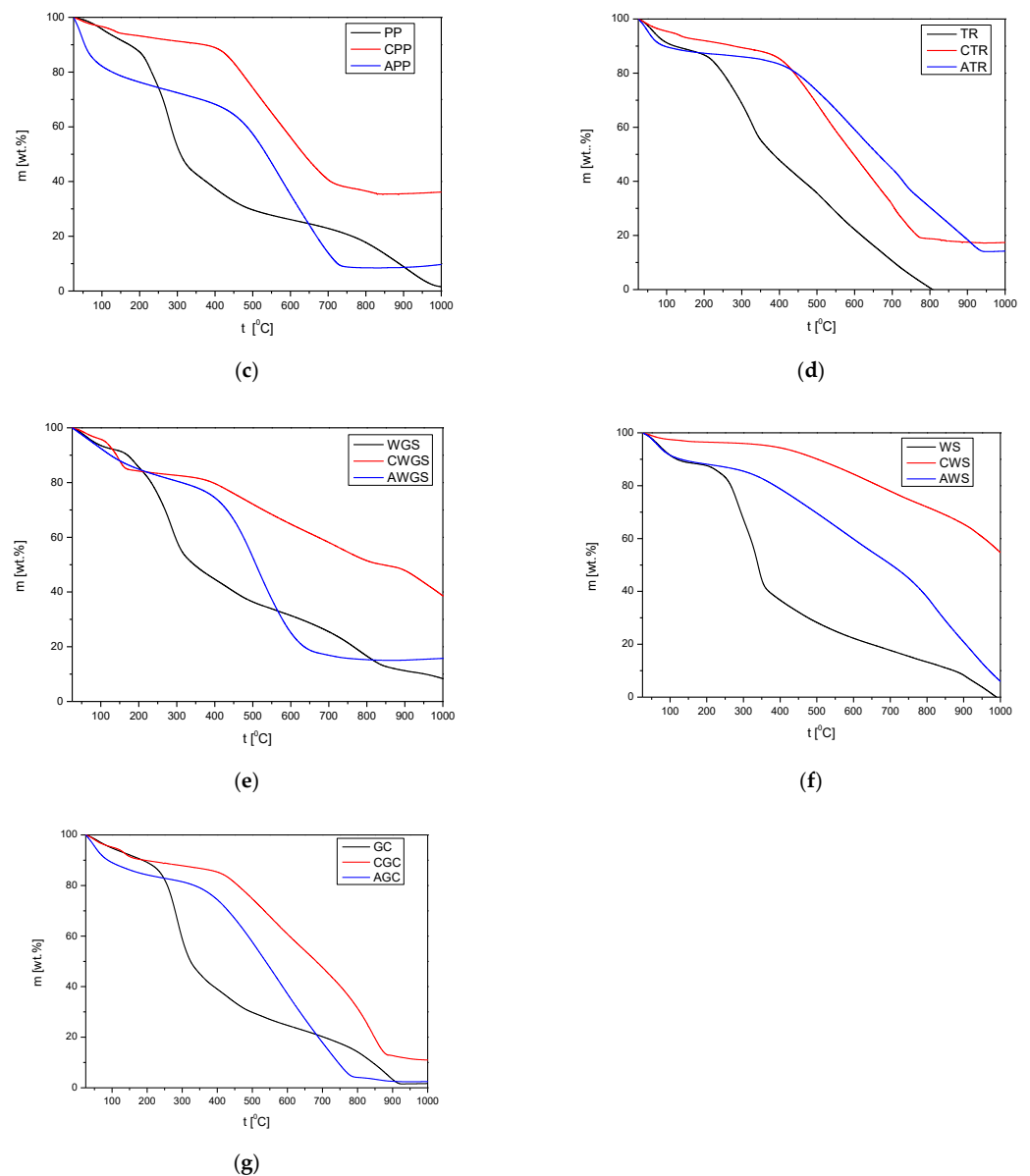


Figure 14. TGA profiles for (a) heavily roasted coffee residue, (b) regular roasted coffee residue, (c) potato peelings, (d) tea residue, (e) walnut green shells, (f) walnut shells, (g) green coffee residue.

The weight loss curves for the carbonized and activated potato peeling sample are very similar (Figure 14c,e,g). Thermal stability is obtained at 650–700 °C, and rapid weight loss occurs between 450 °C and 650 °C.

The course of the curve for the decomposition of the carbonized and activated tea samples is very similar, except that the thermal stability for the carbonized sample is reached at 750 °C, and for the activated one, it is reached at 900 °C.

The course of the curve for the decomposition of the activated green walnut shell sample is similar to that of the activated potato peeling sample. Stability is reached at 650 °C, and the last peak weight loss lasts from 450 °C to 650 °C. For the carbonized sample, weight loss begins at 450 °C with no clear end.

The course of the curve for the decomposition of the carbonized and activated walnut shell samples is similar—no thermal stability.

The course of the curve for the decomposition of the carbonized and activated green coffee samples is very similar, except that the thermal stability for the activated sample is reached at 750 °C, and for the carbonized one, it is reached at 850 °C.

3.2.5. XRD Analysis

The XRD patterns of the samples are shown in Figure 15. The obtained results were compared with those reported in the International Center for Diffraction Data (ICDD). Every sample shows broad peaks at about $2\theta = 24^\circ$ and 44° . These peaks can be related to the typical characteristics of carbon [48]. Along with the modifications carried out, such as carbonization and then activation of organic waste, the intensity of the peaks decreases and smoothing occurs. This is due to the disorder of the carbon. Mallesh et al. showed similar changes in the XRD analysis of an adsorbent they prepared based on the shells of a local nut activated with sodium hydroxide [49]. The broad peak at 24° is associated with the graphite system and represents a highly disordered crystalline structure consisting of both aliphatic side chains and an amorphous carbon structure. Compared to the broad diffuse peak in amorphous carbon, the graphite band at 44° indicates the presence of an aromatic structure. The slight sharp peaks at $2\theta = 32.3^\circ$ can be attributed to the modifications caused by the activation with potassium hydroxide. Reflections like others at $2\theta = 31.2, 44.6, 50.1^\circ$ are characteristic of samples activated with potassium hydroxide. Lahijani et al., who activated the obtained biochar with NaNO_3 , also showed peaks at the above-mentioned degrees [50].

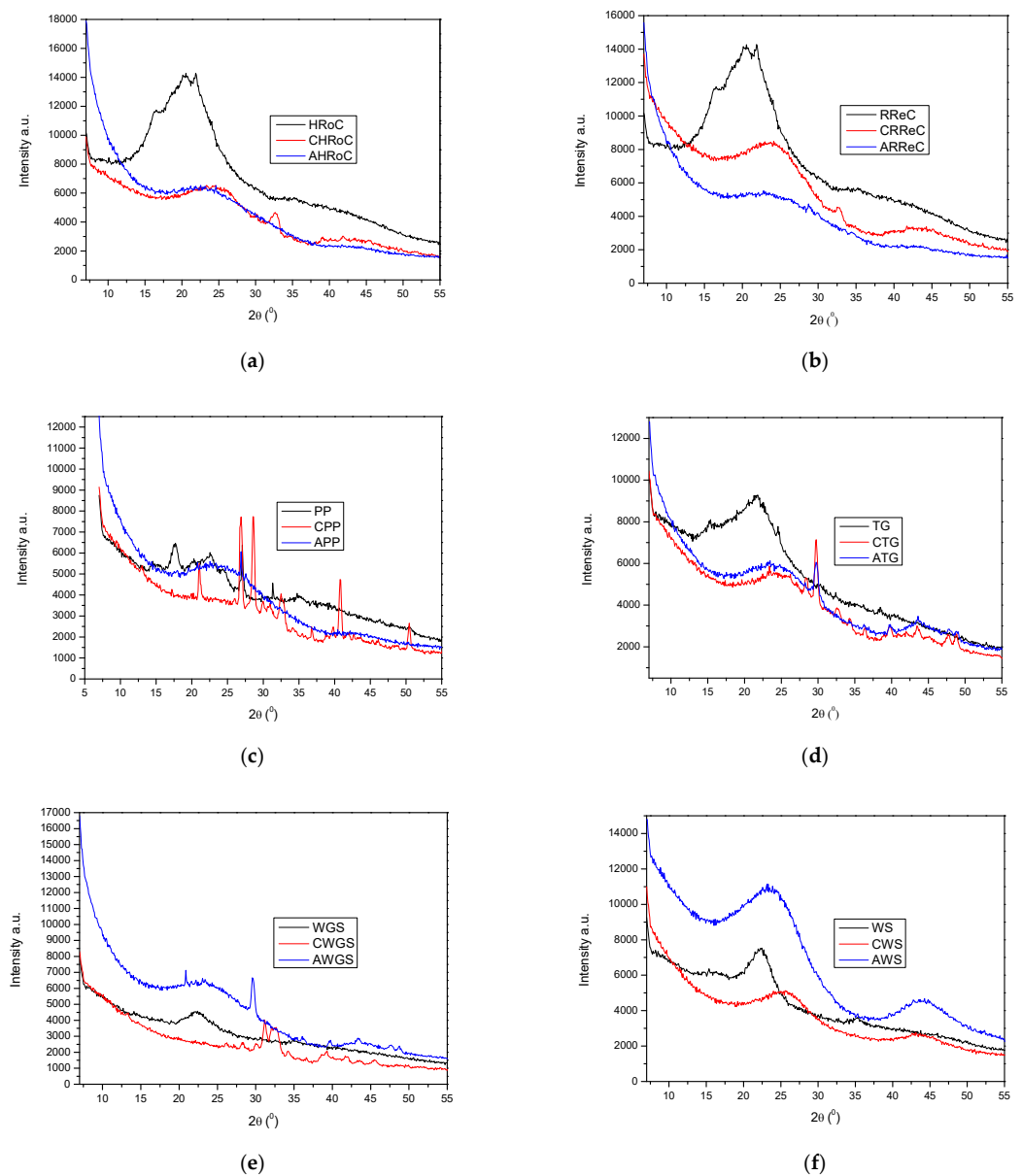
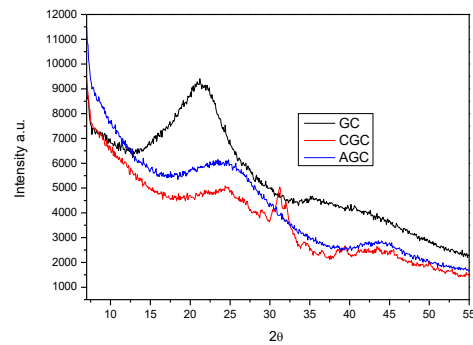


Figure 15. Cont.



(g)

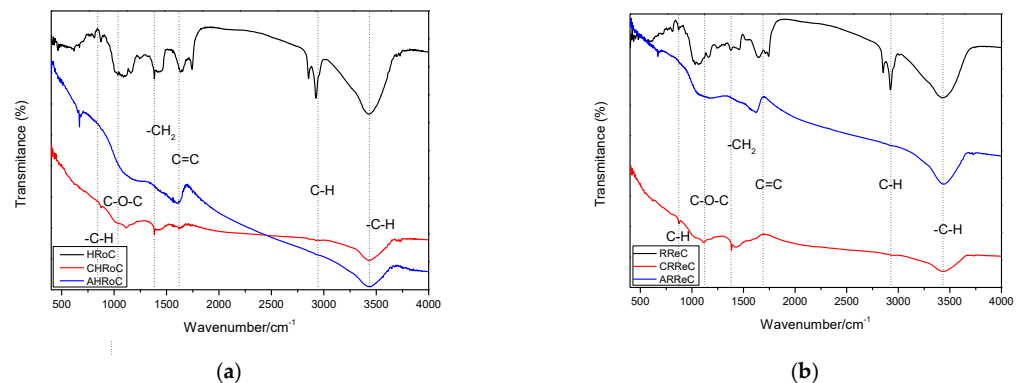
Figure 15. XRD patterns of the samples with (a) heavily roasted coffee residue, (b) regular roasted coffee residue, (c) potato peelings, (d) tea residue, (e) walnut green shells, (f) walnut shells, (g) green coffee residue.

3.2.6. FT-IR Analysis

Figure 16a–g show the FTIR spectra samples of organic waste carried out on biomass and samples after modification of organic waste (after process carbonization and activation). Each of the spectra has several characteristic bands in close positions. The wide transmission bandwidth at 3315 cm^{-1} is attributed to -O-H stretching. Another peak in the spectra around 2900 cm^{-1} is the stretching bond -C-H [35]. The peak at 1700 cm^{-1} corresponds to the C=O stretching skeleton and 1024 cm^{-1} corresponds to asymmetric C-O-C stretching vibrations. The peak at 750 cm^{-1} visible in some spectra is the -C-H bond [51]. This bond is visible for samples (ARoC, AReC, ATG, AWGS) that are enhanced by increasing the mass ratio of KOH to biomass. It indicates that the activation of KOH promotes the graphitization of activated carbons [29].

All spectra show that in pure biomass samples there are bands before 3000 cm^{-1} corresponding to aliphatic groups -C-H . The spectra of pure biomass are characterized by greater variability, and with a greater number of peaks in each spectrum, along with the introduced modifications, the spectrum becomes smoother.

Table 8 summarizes the activation conditions and the most important textural parameters for the samples of this article and those obtained for samples from similar precursors. The results obtained for specific surface area (S_{BET}), pore volume (V_p), micropore volume (W_o), and average micropore width (L_o) are better for the samples in this article except for the sample of activated walnut shells. Not all parameters could be compared nor could all precursors. There is a lack of data in the literature that would allow a complete comparison of these parameters.



(a)

(b)

Figure 16. Cont.

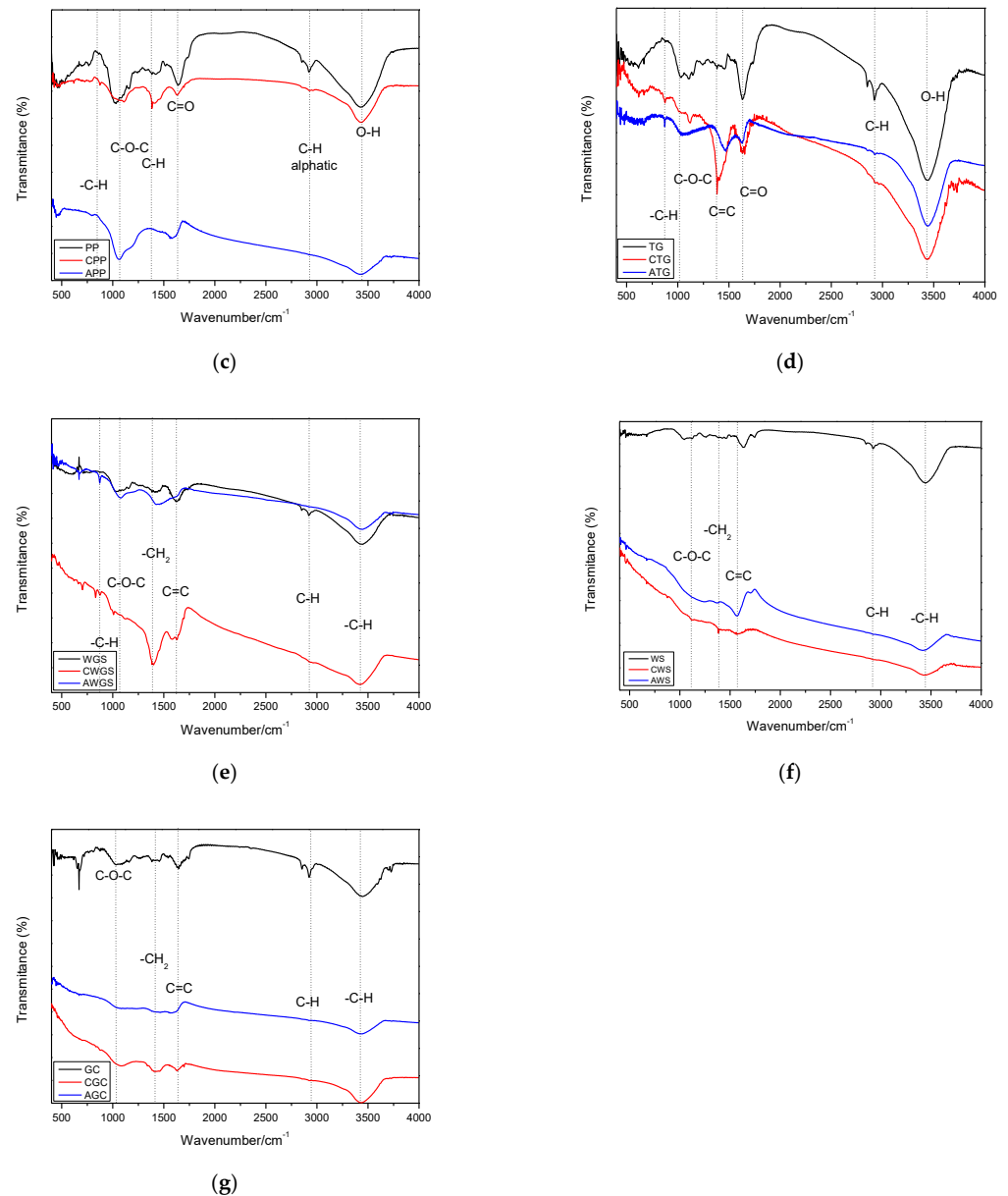


Figure 16. FTIR spectrum of organic waste and the products received with (a) heavily roasted coffee residue, (b) regular roasted coffee residue, (c) potato peelings, (d) tea residue, (e) walnut green shells, (f) walnut shells, (g) green coffee residue.

It should be noted that the values given in this work are higher than those available in the literature for analogous carbons. Only the bioadsorbents obtained by Boudrahem and others from coffee waste under the same activation conditions have a slightly higher specific surface area but a smaller pore volume.

The results also prove that the potassium hydroxide used is a better activator than other substances. None of the other activators used, such as phosphoric acid(V), zinc chloride, and others, allowed for such a strong development of the porous structure of bioadsorbents.

The average micropore values indicate high crystallization of the samples. This proves the potential use of these bioadsorbents for pollutant capture purposes.

Table 8. Comparison of the activation parameters and the most important textural parameters for the samples in this article with the literature data.

| Precursor | Activation Conditions | | Textural Parameters | | | | Ref. |
|----------------|--|--------|--------------------------------------|-------------------------------------|-------------------------------------|---------------------|------------|
| | Activation Precursor | T [°C] | S _{BET} [m ² /g] | V _p [cm ³ /g] | W _o [cm ³ /g] | L _o [nm] | |
| Coffee grounds | H ₃ PO ₄ | 450 | 925 | 0.718 | n/a | n/a | [52] |
| Coffee grounds | CO ₂ | 700 | 593 | 0.24 | 0.24 | 0.8 | [23] |
| Coffee grounds | Steam | 800 | 981.12 | 1.03 | n/a | 4.19 | [53] |
| Coffee residue | H ₃ PO ₄ | 600 | 1003 | 0.618 | n/a | n/a | [54] |
| Coffee residue | KOH | 700 | 1624 | 0.662 | n/a | n/a | [35] |
| Coffee residue | KOH | 700 | 1580 | 0.84 | 0.5 | 0.96 | This study |
| Waste potato | ZnCl ₂ | 600 | 1357 | 1.065 | n/a | n/a | [42] |
| Waste potato | KOH | 700 | 1383 | 0.736 | 0.234 | n/a | [55] |
| Waste potato | KOH | 700 | 1604 | 0.65 | 0.32 | 1.36 | This study |
| Tea residue | C ₂ H ₃ O ₂ K | 800 | 820 | 0.219 | n/a | n/a | [56] |
| Tea residue | KOH | 500 | 256.45 | n/a | n/a | n/a | [57] |
| Tea residue | KOH | 700 | 564 | 0.25 | 0.12 | 0.86 | This study |
| Walnut shell | H ₃ PO ₄ | 500 | 789 | 0.304 | n/a | n/a | [58] |
| Walnut shell | KOH | 700 | 416 | 0.2 | 0.18 | 0.86 | This study |

4. Conclusions

The literature currently lacks information on changes in the specific surface area of organic waste before modifying the structure of the material. Researchers focus on examining already obtained bioadsorbents, without comparing their properties before modification. Moreover, articles often focus on one type of waste, which makes it difficult to compare the properties of waste obtained under similar conditions.

This article carried out research at all stages of structural modifications. Material tests were carried out both for non-activated materials, after the carbonization process and after the activation process.

As a result of the work carried out to carbonize and activate seven different types of waste biomass, the most effective adsorbent turned out to be a bioadsorbent derived from roasted coffee residues. After activation, this adsorbent had a well-developed specific surface area of 1580 m²/g (in relation to the range of 593–1624 m²/g from the literature), a visible structure and a pore volume of 0.84 cm³/g. A bioadsorbent from potato peels with a surface area of 1604 m²/g and a pore volume of 0.65 cm³/g turned out to be an effective sorbent.

The worst starting material for obtaining a bioadsorbent was walnut shell, as evidenced by the surface area of 416 m²/g.

Analyzes of raw biomass materials as well as the intermediate product before the final preparation of the bioadsorbent also showed: a large weight loss and a change in structure towards porosity in the carbonization phase. Only chemical activation of KOH resulted in a significant increase in the surface area, which confirms that chemical activation is an effective activation method.

Author Contributions: Conceptualization, I.M.-K. and M.S.; methodology, M.S.; software, M.S.; validation, M.S. and D.W.; formal analysis, I.M.-K.; data curation, M.S.; writing—original draft preparation, M.S.; writing—review and editing, I.M.-K. and D.W.; visualization, M.S.; supervision, I.M.-K. and D.W. All authors have read and agreed to the published version of the manuscript.

Funding: The scientific research was funded by the statute subvention of Czestochowa University of Technology, Faculty of Infrastructure and Environment.

Institutional Review Board Statement: Not applicable.

Informed Consent Statement: Not applicable.

Data Availability Statement: Data are contained within the article.

Conflicts of Interest: The authors declare no conflict of interest.

References

1. Municipal Waste by Waste Management Operations, Eurostat. Available online: https://ec.europa.eu/eurostat/databrowser/view/env_wasmun/default/table?lang=en (accessed on 1 December 2023).
2. Recycling: The Seventh Resource Manifesto, Global Recycling Day. 18 March 2018. Available online: <https://www.bir.org/publications/facts-figures/item/recycling-the-seventh-resource-manifesto> (accessed on 9 May 2022).
3. Directive (EU) 2018/851 of the European Parliament and of the Council of 30 May 2018 Amending Directive 2008/98/EC on Waste. Available online: <https://eur-lex.europa.eu/legal-content/PL/TXT/?uri=CELEX:32018L0851> (accessed on 15 March 2024).
4. National Waste Management Plan 2028. Available online: <https://bip.mos.gov.pl/strategie-plany-programy/krajowy-plan-gospodarki-odpadami/> (accessed on 11 March 2023).
5. *Podstawy Gospodarki Odpadami*; Publ. PWN, Ed. 6; Czesława Rosik-Dulkowska: Warsaw, Poland, 2023.
6. European Parliament, Waste Management in the EU: Facts and Figures (Infographic), Last Update: 17/11/2023. Available online: <https://www.europarl.europa.eu/topics/en/article/20181212STO21610/plastic-waste-and-recycling-in-the-eu-facts-and-figures> (accessed on 13 February 2024).
7. Central Statistical Office. *Environmental Protection 2022, Statistical Analyses*; Central Statistical Office: Warsaw, Poland, 2022.
8. Green Economy, A Ton of Coffee Grounds Worth PLN 4000. Euro. Available online: <https://zielonagospodarka.pl/tona-fusow-pokawie-warta-4-tys-euro-start-up-ecobean-pracuje-nad-uruchomieniem-kawowej-biorafinerii-6397> (accessed on 13 May 2023).
9. Center for Good Therapy, to Drink Tea or Not to Drink. Available online: <https://www.centrumdobrejterapii.pl/materialy/herbata-pic-czy-nie-pic/> (accessed on 21 April 2023).
10. Institute for the Development of Ecological Thought, Potato—The Undisputed Leader Among Vegetables on Polish Tables. Available online: <https://irme.pl/ziemniak-niekwestionowany-krol-posrod-warzyw-na-polskich-stolach/> (accessed on 13 April 2023).
11. Obeng, G.Y.; Amoah, D.Y.; Opoku, R.; Sekyere, C.K.; Adjei, E.A.; Mensah, E. Coconut wastes as bioresources for sustainable energy: Quantifying waste, calorific value and emissions in Ghana. *Energies* **2020**, *13*, 2178. [CrossRef]
12. Spasówka, E. The Goodyear corporation aims to double the use of silica from rice husks in 2021. *Polimery* **2021**, *66*, 146.
13. Wang, R.; Wang, G. Acceleration effect of rice husk ash on hydration of styrene-acrylic ester/cement composite pastes. *Cement Wapno Beton* **2018**, *23*, 5. [CrossRef]
14. Meneguzzo, F.; Brunetti, C.; Fidalgo, A.; Ciriminna, R.; Delisi, R.; Albanese, L.; Zabini, F.; Gori, A.; Nascimento, L.B.D.S.; De Carlo, A.; et al. Real-scale integral valorization of waste orange peel via hydrodynamic cavitation. *Processes* **2019**, *7*, 581. [CrossRef]
15. Decofire, How to Use Coffee Grounds? Available online: <https://decofire.pl/blog/jak-wykorzystac-fusy-z-kawy> (accessed on 9 March 2024).
16. Chen, J.; Yang, J.; Hu, X.; Li, Z.; Shen, S.; Radosz, M.; Fan, M. Enhanced CO₂ capture capacity of nitrogen-doped biomass-derived porous carbons. *ACS Sustain. Chem. Eng.* **2016**, *4*, 1439–1445. [CrossRef]
17. Ello, A.S.; Souza, L.K.C.; Trokorey, A.; Jaroniec, M. Coconut shell-based microporous carbons for CO₂ capture. *Microporous Mesoporous Mater.* **2013**, *180*, 280–283. [CrossRef]
18. He, S.; Chen, G.; Xiao, H.; Shi, G.; Ruan, C.; Ma, Y.; Dai, H.; Yuan, B.; Chen, X.; Yang, X. Facile preparation of N-doped activated carbon produced from rice husk for CO₂ capture. *J. Colloid Interface Sci.* **2021**, *582*, 90–101. [CrossRef]
19. Li, D.; Ma, T.; Zhang, R.; Tian, Y.; Qiao, Y. Preparation of porous carbons with high low-pressure CO₂ uptake by KOH activation of rice husk char. *Fuel* **2015**, *139*, 68–70. [CrossRef]
20. Ouzzine, M.; Serafin, J.; Sreńscek-Nazzal, J. Single step preparation of activated biocarbons derived from pomegranate peels and their CO₂ adsorption performance. *J. Anal. Appl. Pyrolysis* **2021**, *160*, 105338. [CrossRef]
21. Serafin, J.; Narkiewicz, U.; Morawski, A.W.; Wróbel, R.J.; Michalkiewicz, B. Highly microporous activated carbons from biomass for CO₂ capture and effective micropores at different conditions. *J. CO₂ Util.* **2017**, *18*, 73–79. [CrossRef]
22. Querejeta, N.; Gil, M.V.; Rubiera, F.; Pevida, C. Sustainable coffee-based CO₂ adsorbents: Toward a greener production via hydrothermal carbonization. *Greenh. Gases Sci. Technol.* **2018**, *8*, 309–323. [CrossRef]
23. Plaza, M.G.; González-Vázquez, M.P.; Pevida, C.; Pis, J.J.; Rubiera, F. Valorisation of spent coffee grounds as CO₂ adsorbents for postcombustion capture applications. *Appl. Energy* **2012**, *99*, 272–279. [CrossRef]
24. Tubers. PWN Dictionary of Biological Terms. Available online: <https://sjp.pwn.pl/sjp/bulwa;2446675.html> (accessed on 7 March 2022).
25. Fonseca, D.C. Visionary leadership and the case of Dilmah. *Sri Lankan J. Manag.* **2009**, *14*, 1–16. [CrossRef]
26. Zdyb, H. *Walnut*; National Agricultural and Forestry Publishing House: Warsaw, Poland, 2009; p. 182. ISBN 978-83-09-01042-5.
27. *PN-EN ISO 18134-1*; Solid Biofuels. Determination of Moisture Content. Dryer Method. Vol. 1. Total Moisture. Reference Method. ISO: Geneva, Switzerland, 2015. Available online: <https://www.iso.org/standard/61538.html> (accessed on 7 March 2023).
28. *PN-EN ISO 16948:2015-07*; Determination of Total Carbon, Hydrogen and Nitrogen Content in Solid Biofuels. System Cyfrowej Sprzedazy Produktow Usług. ISO: Geneva, Switzerland, 2015. Available online: <https://www.iso.org/obp/ui/#iso:std:iso:16948:ed-1:v1:en> (accessed on 7 March 2023).

29. Gan, Y.X. Activated Carbon from Biomass Sustainable Sources. *C—J. Carbon Res.* **2021**, *7*, 39. [[CrossRef](#)]
30. Gil, M.V.; Riaza, J.; Álvarez, L.; Pevida, C.; Rubiera, F. Biomass devolatilization at high temperature under N₂ and CO₂: Char morphology and reactivity. *Energy* **2015**, *91*, 655–662. [[CrossRef](#)]
31. Ukanwa, K.S.; Patchigolla, K.; Sakrabani, R.; Anthony, E.; Mandavgane, S. A review of chemicals to produce activated carbon from agricultural waste biomass. *Sustainability* **2019**, *11*, 6204. [[CrossRef](#)]
32. Kim, M.J.; Choi, S.W.; Kim, H.; Mun, S.; Lee, K.B. Simple synthesis of spent coffee ground-based microporous carbons using K₂CO₃ as an activation agent and their application to CO₂ capture. *Chem. Eng. J.* **2020**, *397*, 125404. [[CrossRef](#)]
33. Hojjati-Najafabadi, A.; Farahbakhsh, E.; Gholamalian, G.; Feng, P.; Davar, F.; Aminabhavi, T.M.; Vasseghian, Y.; Kamyab, H.; Rahimi, H. Controllable synthesis of nanostructured flower-like cadmium sulfides for photocatalytic degradation of methyl orange under different light sources. *J. Water Process. Eng.* **2024**, *59*, 105002. [[CrossRef](#)]
34. Yousaf, B.; Gujian, L.; Qumber, A.; Ruwei, W.; Ali, M.U.; Ullah, H.; Liu, R.; Zhou, C. Systematic investigation on combustion characteristics and emission-reduction mechanism of potentially toxic elements in biomass-and biochar-coal co-combustion systems. *Appl. Energy* **2017**, *208*, 142–157. [[CrossRef](#)]
35. Bader, N.; Abdelmottaleb, O. CO₂ activation of olive bagasse for hydrogen storage. *Environ. Prog. Sustain. Energy* **2017**, *36*, 315–324. [[CrossRef](#)]
36. McEnaney, B. Estimation of the dimensions of micropores in active carbons using the Dubinin-Radushkevich equation. *Carbon* **1987**, *25*, 69–75. [[CrossRef](#)]
37. Gomis-Berenguer, A.; Iniesta, J.; Moro, A.; Maurino, V.; Lima, J.C.; Ania, C.O. Boosting visible light conversion in the confined pore space of nanoporous carbons. *Carbon* **2016**, *96*, 98–104. [[CrossRef](#)]
38. Rouzitalab, Z.; Maklavany, D.M.; Jafarinejad, S.; Rashidi, A. Lignocellulose-based adsorbents: A spotlight review of the effective parameters on carbon dioxide capture process. *Chemosphere* **2020**, *246*, 125756. [[CrossRef](#)] [[PubMed](#)]
39. Abuelnoor, N.; AlHajaj, A.; Khaleel, M.; Vega, L.F.; Abu-Zahra, M.R.M. Activated carbons from biomass-based sources for CO₂ capture applications. *Chemosphere* **2021**, *282*, 131111. [[CrossRef](#)] [[PubMed](#)]
40. Travis, W.; Srinivas, G.; Zhengxiao, G. Superior CO₂ adsorption from waste coffee ground derived carbons. *RSC Adv.* **2015**, *5*, 29558–29562. [[CrossRef](#)]
41. Zhang, Z.; Luo, X.; Liu, Y.; Zhou, P.; Ma, G.; Lei, Z.; Lei, L. A low cost and highly efficient adsorbent (activated carbon) prepared from waste potato residue. *J. Taiwan Inst. Chem. Eng.* **2015**, *49*, 206–211. [[CrossRef](#)]
42. Thommes, M.; Kaneko, K.; Neimark, A.V.; Olivier, J.P.; Rodriguez-Reinoso, F.; Rouquerol, J.; Sing, K.S.W. Physisorption of gases, with special reference to the evaluation of surface area and pore size distribution (IUPAC Technical Report). *Pure Appl. Chem.* **2015**, *87*, 1051–1069. [[CrossRef](#)]
43. Hojjati-Najafabadi, A.; Esfahani, P.N.; Davar, F.; Aminabhavi, T.M.; Vasseghian, Y. Adsorptive removal of malachite green using novel GO@ZnO-NiFe₂O₄-αAl₂O₃ nanocomposites. *Chem. Eng. J.* **2023**, *471*, 144485. [[CrossRef](#)]
44. Mohammed, A.; Abdullah, A. Scanning electron microscopy (SEM): A review. In Proceedings of the 2018 International Conference on Hydraulics and Pneumatics—HERVEX, Băile Govora, Romania, 7–9 November 2018; pp. 7–9, ISSN 1454-8003.
45. Yargicoglu, E.N.; Sadasivam, B.Y.; Reddy, K.R.; Spokas, K. Physical and chemical characterization of waste wood derived biochars. *Waste Manag.* **2015**, *36*, 256–268. [[CrossRef](#)]
46. Xu, Y.; Chen, B. Investigation of thermodynamic parameters in the pyrolysis conversion of biomass and manure to biochars using thermogravimetric analysis. *Bioresour. Technol.* **2013**, *146*, 485–493. [[CrossRef](#)]
47. Zhou, W.; Apkarian, R.; Wang, Z.L.; Joy, D. Fundamentals of scanning electron microscopy (SEM). *Scanning Microsc. Nanotechnol. Tech. Appl.* **2006**, 1–40. [[CrossRef](#)]
48. Wang, Z.; Zhang, X.; Liu, X.; Lv, M.; Yang, K.; Meng, J. Co-gelation synthesis of porous graphitic carbons with high surface area and their applications. *Carbon* **2011**, *49*, 161–169. [[CrossRef](#)]
49. Mallesh, D.; Anbarasan, J.; Kumar, P.M.; Upendar, K.; Chandrashekar, P.; Rao, B.V.S.K.; Lingaiah, N. Synthesis, characterization of carbon adsorbents derived from waste biomass and its application to CO₂ capture. *Appl. Surf. Sci.* **2020**, *530*, 147226. [[CrossRef](#)]
50. Lahijani, P.; Mohammadi, M.; Mohamed, A.R. Metal incorporated biochar as a potential adsorbent for high capacity CO₂ capture at ambient condition. *J. CO₂ Util.* **2018**, *26*, 281–293. [[CrossRef](#)]
51. Singh, G.; Lakhi, K.S.; Ramadass, K.; Kim, S.; Stockdale, D.; Vinu, A. A combined strategy of acid-assisted polymerization and solid state activation to synthesize functionalized nanoporous activated biocarbons from biomass for CO₂ capture. *Microporous Mesoporous Mater.* **2018**, *271*, 23–32. [[CrossRef](#)]
52. Reffas, A.; Bernardet, V.; David, B.; Lehocine, M.B.; Dubois, M.; Batisse, N.; Duclaux, L. Carbons prepared from coffee grounds by H₃PO₄ activation: Characterization and adsorption of methylene blue and Nylosan Red N-2RBL. *J. Hazard Mater.* **2010**, *175*, 779–788. [[CrossRef](#)] [[PubMed](#)]
53. Adan-Mas, A.; Alcaraz, L.; Arévalo-Cid, P.; López-Gómez, F.A.; Montemor, F. Coffee-derived activated carbon from second biowaste for supercapacitor applications. *Waste Manag.* **2021**, *120*, 280–289. [[CrossRef](#)] [[PubMed](#)]
54. Boudrahem, F.; Soualah, A.; Aissani-Benissad, F. Pb (II) and Cd (II) removal from aqueous solutions using activated carbon developed from coffee residue activated with phosphoric acid and zinc chloride. *J. Chem. Eng. Data* **2011**, *56*, 1946–1955. [[CrossRef](#)]
55. Idrees, M.; Rangari, V.; Jeelani, S. Sustainable packaging waste-derived activated carbon for carbon dioxide capture. *J. CO₂ Util.* **2018**, *26*, 380–387. [[CrossRef](#)]

56. Auta, M.; Hameed, B.H. Preparation of waste tea activated carbon using potassium acetate as an activating agent for adsorption of Acid Blue 25 dye. *Chem. Eng. J.* **2011**, *171*, 502–509. [[CrossRef](#)]
57. Rattanaphan, S.; Rungrotmongkol, T.; Kongsune, P.P. Biogas improving by adsorption of CO₂ on modified waste tea activated carbon. *Renew. Energy* **2020**, *145*, 622–631. [[CrossRef](#)]
58. Moreno-Barbosa, J.J.; López-Velandia, C.; Maldonado, A.D.P.; Giraldo, L.; Loreno-Piraján, J.C. Removal of lead (II) and zinc (II) ions from aqueous solutions by adsorption onto activated carbon synthesized from watermelon shell and walnut shell. *Adsorp.* **2013**, *19*, 675–685. [[CrossRef](#)]

Disclaimer/Publisher’s Note: The statements, opinions and data contained in all publications are solely those of the individual author(s) and contributor(s) and not of MDPI and/or the editor(s). MDPI and/or the editor(s) disclaim responsibility for any injury to people or property resulting from any ideas, methods, instructions or products referred to in the content.